Eur. Phys. J. Plus (2024) 139:3
https://doi.org/10.1140/epjp/s13360-023-04782-9

THE EUROPEAN PHYSICAL JOURNAL PLUS

Regular Article

Influence of hydrostatic pressure and temperature on the optical responses of asymmetric triple quantum wells

A. Salman Durmuslar[1,a], **H. Dakhlaoui**[2,3,b], **E. B. Al**[4,c], **F. Ungan**[4,d]

[1] Department of Electrical and Electronic Engineering, Faculty of Engineering, Piri Reis University, 34940 Istanbul, Turkey
[2] Nanomaterials Technology Unit, Basic and Applied Scientific Research Center (BASRC), College of Science of Dammam, Imam Abdulrahman Bin Faisal University, P. O. Box 1982, 31441 Dammam, Saudi Arabia
[3] Department of Physics, College of Sciences for Girls, Imam Abdulrahman Bin Faisal University, Dammam, Saudi Arabia
[4] Department of Physics, Faculty of Science, Sivas Cumhuriyet University, 58140 Sivas, Turkey

Received: 14 September 2023 / Accepted: 9 December 2023

Abstract The work presents the effects of hydrostatic pressure and temperature on the electronic spectra as well as on the optical responses of parabolically shaped asymmetric triple quantum wells formed between the GaAs/$Al_{0.3}Ga_{0.7}As$ heterostructures. The electronic structure of the configuration is obtained by iteratively solving the Schrödinger equation within effective mass and envelope wave function approximations. Optical properties are calculated within the compact density matrix approach framework. The results in this study show that increasing hydrostatic pressure field leads to small redshifts on the total optical absorption coefficient, relative refractive index change, nonlinear optical correction, and second and third harmonic generations, while temperature augmentation causes significant redshifts in these optical properties.

1 Introduction

Electronic and optical properties of quantum structures remain the interest due to their wide range of applications in optoelectronic devices. With the advancing studies, different confining potentials within semiconductor heterostructures are introduced to examine the diverse tuning properties for the intersubband transitions and related optical properties [1–11]. The devolopments in the fabrication processes also made it possible to produce the desired confining potentials and contribute to this research area [12–18].

Single or multiple quantum wells (QWs) with different external perturbations such as electric, magnetic, and laser fields have been examined due to their strong and tunable confinement potential characteristics. Altering the potential by external probes brings changes in the electronic and therefore in the optical spectra. Knowing the relations between electronic and optical properties allows choosing suitable conditions for practical applications. Like other external agents, hydrostatic pressures and temperatures can be used to modulate the transition energies and related wavefunctions of confined particles [19–32]. When the varying hydrostatic pressure and temperature applied to the heterostructure, the gap between the energies of the barrier and well region of the heterostructure alters. Therefore, these changes modify the depth of the potential wells, the effective mass of conduction electron, and the relative dielectric constant of the system. Besides, the increase in the hydrostatic pressure acts on the well width of the system.

The roles of hydrostatic pressure and temperature on the electronic and optical properties of QWs have been investigated in several studies. The influence of hydrostatic pressure on the binding energy of donor impurity is evaluated for different shapes of QWs; such as rectangular QWs [19–22], square and parabolic QWs [23], and symmetrical double QWs [24]. In addition to the hydrostatic pressure, the effect of temperature is included in the donor binding energies for asymmetrical square QWs [25], Pöschl–Teller QW [26], InP/InGaAs/InP square QW [27], finite QW [28], cylindrical quantum well wires [29], and double QWs [30]. The effects of these fields on the shallow impurity-related optical absorption character are surveyed for single and double QWs [31] and for symmetrical GaAs double QWs [32].

The responses of the total optical absorption coefficients (TOACs) and relative refractive index changes (RRICs) to the hydrostatic pressure and temperature are searched for modulation-doped QWs [33], square and graded QWs [34], symmetric double semi-V-shaped QWs [35], asymmetrical Gaussian potential QWs [36], Morse QW [37], and zigzag QW [38]. Ungan and coworkers included the external electric field to the pressure and temperature fields and examined the combined effects of these fields on the TOACs

[a] e-mail: asdurmuslar@pirireis.edu.tr (corresponding author)
[b] e-mail: hbaldkhlaen@iau.edu.sa
[c] e-mail: emrebahadiral@hotmail.com
[d] e-mail: fungan@cumhuriyet.edu.tr

Published online: 02 January 2024

and RRICs of a graded QW [39]. Furthermore, the role of laser fields together with pressure and temperature fields on the TOACs and RRICs is investigated for parabolic QW [40], symmetric and asymmetric n-type double delta-doped QWs [41] and asymmetric double QWs [42]. In addition to these studies on the QWs, the influences of hydrostatic pressure and temperature on the nonlinear optical rectification (NOR), and second and third harmonic generations (SHGs and THGs) are examined in some studies. For instance, the influence of refered fields on the SHG coefficients are examined for a zigzag QW [38] and asymmetric double semi-parabolic QWs [43]. The variations on the NOR, SHG, and THG coefficients with the hydrostatic pressure and temperature fields are investigated for a Gaussian potential QW [44], Morse QW [45], and Kratser-Fues confined QW [46].

In this work, we analyzed the effect of hydrostatic pressure and temperature on the TOACs, RRICs, NOR, SHG, and THG coefficients for an asymmetric triple QW. The modulations on the pressure and temperature alter the intersubband transitions and optical spectra; thereby contribute to the research on optoelectronic devices such as solar cells, photo-detectors, laser diodes, and transistors [47–49]. For that, we first obtained the energy levels and corresponding energy wave functions. Then we studied the optical susceptibilities by changing the referred agents. The lack of study on the optical properties with that type of asymmetric triple QWs is the main motivation for us. In the coming sections, we introduced the theoretical part of this study, served the results and discussions on the subject, and composed a summary.

2 Theory

In this study, we worked with a QWs structure shaped with the asymmetric combination of three different potential functions formed within GaAs/AlGaAs heterostructures. We have investigated the role of hydrostatic pressure and temperature on the electronic spectra and optical properties of a conduction band electron. The Hamiltonian operator-$\widehat{H}$, for an electron confined within a potential function in the z direction of the cartesian coordinate system, is given by,

$$\widehat{H} = -\frac{\hbar^2}{2m^*(P,T)}\nabla^2 + V(z,P,T). \tag{1}$$

Here $m^*(p,\ T)$ is the effective mass of the conduction band electron as a function of hydrostatic pressure-p and temperature-T. $V(z,\ p,\ T)$ represents the spatial extension of confinement potential modulated with hydrostatic pressure and temperature. When the varying hydrostatic pressure and temperature applied to the system, the band gap energy between heterostructures, i.e., the depth of potential barrier as well as the widths of the wells and the effective mass of the system will be impressed. In this instance, effective mass of electron can be calculated by the formula given below:

$$m^*(p,T) = \frac{m_0}{1 + E_p^{\Gamma}\left[\frac{2}{E_g^{\Gamma}(p,T)} + \frac{1}{E_g^{\Gamma}(p,T)+\Delta_0}\right]} \tag{2}$$

where m_0 is the mass of a free electron, $E_p^{\Gamma} = 7.51eV$ is the momentum-associated energy between GaAs/AlGaAs semiconductors at Γ point and $\Delta_0 = 0.341$eV is the spin–orbit splitting energy of the valance band of GaAs. $E_g^{\Gamma}(p,\ T)$ is the hydrostatic pressure and temperature-dependent energy gap at the Γ point of GaAs and can be explained as:

$$E_g^{\Gamma}(p,T) = E_g^{\Gamma}(0,T) + bp - cp^2, \tag{3}$$

where $E_g^{\Gamma}(0,\ T)$ is the temperature-dependent gap energy when no pressure field is acting and changes with temperature as $E_g^{\Gamma}(0,\ T) = 1.519 - \left[\frac{5.405\times10^{-4}T^2}{T+204}\right]$. The influence of hydrostatic pressure has included this gap energy with factors, $b = 1.26 \times 10^{-2}e$V/kbar and $c = 3.77 \times 10^{-5}$eV/kbar^2.

The spatial distribution of examined confinement potential includes different parabolic-like potential forms placed asymmetrically (see Fig. 1), as proposed by Zhang and Yuan and given as follows [50]:

$$V(z,p,T) = V_0(p,T)\begin{cases} \frac{2}{L_L^2}\left(z + L_B + \frac{(L_M+L_L)}{2}\right)^2, -\left(L_L + L_B + \frac{L_M}{2}\right) \le z \le -\left(L_B + \frac{L_M}{2}\right) \\ -\frac{2}{L_M^2}z^2 + \frac{1}{2}, -\frac{L_M}{2} \le z \le 0 \\ \frac{2}{L_M^2}z^2, 0 \le z \le \frac{L_M}{2} \\ -\frac{2}{L_R^2}\left(z - L_B - \frac{(L_M+L_R)}{2}\right)^2 + \frac{1}{2}, \frac{L_M}{2} + L_B \le z \le \frac{L_M}{2} + L_B + L_R \\ 1, elsewhere \end{cases}, \tag{4}$$

where $V_0(p,\ T)$ is the height of the potential barrier and L_L, L_R, and L_M represent the widths of left, right, and middle wells, respectively. The length of the barrier region between each well configuration is represented by L_B. The aluminum (Al) ratio in the barrier region, changes the depth of the barrier and acts on the energy differences between the well and barrier materials. In this study, we fixed Al contamination-x to 0.3. With these conditions, the band gap difference at the Γ-point varies with hydrostatic pressure and temperature as follows:

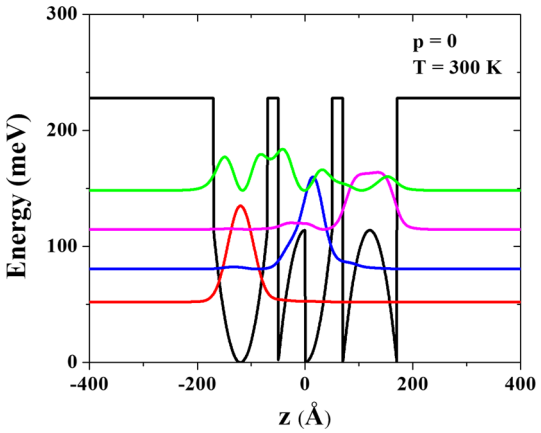

Fig. 1 Potential profile of asymmetric triple QWs with four lowest-lying energy levels and associated wavefunction probabilities at 300 K temperature while no pressure is acting

$$\Delta E_g^{\Gamma}(0.3, p, T) = 0.3798 - 0.39 \times 10^{-3} p - 0.345 \times 10^{-4} T \tag{5}$$

The band gap energy difference and depth of the potential have been connected with a band offset parameter-Q_c, and it is taken as 0.6 for GaAs/AlGaAs heterostructures [37, 51]. Therefore, the depth of the potential barrier can be defined as below:

$$(p, T) = 0.6\Delta E_g^{\Gamma}(0.3, p, T). \tag{6}$$

In addition to the changes in the effective mass and depth of the potential wells, the length of well regions and relative dielectric permittivity between heterostructures will be influenced by the changes in pressure and temperature. The effect of pressure on the length of the well region-L_W can be formulated as,

$$L_w(p) = L_W[1 - (S_{11} + 2S_{12})p], \tag{7}$$

where $S_{11} = 1.16 \times 10^{-3}\text{kbar}^{-1}$ and $S_{12} = -3.70 \times 10^{-4}\text{kbar}^{-1}$.

The dependency of the relative dielectric constant on the pressure and temperature is given by

$$\varepsilon_d(p, T) = \begin{cases} 12.74\exp\left[-1.67 \times 10^{-3} p\right]\exp\left[9.4 \times 10^{-5}(T - 75.6)\right], for T \leq 200K \\ 13.18\exp\left[-1.73 \times 10^{-3} p\right]\exp\left[20.4 \times 10^{-5}(T - 300)\right], for T > 200K \end{cases} \tag{8}$$

and $\varepsilon_b(0.3,\ p,\ T) = \varepsilon_d(p,\ T) - 0.936$ [23, 33].

To get the subband energy levels and corresponding electronic wave functions for the QW system, we first solved the introduced Hamiltonian within the diagonalization method. In that method, the base eigenfunctions-$\phi_n(z)$ are expanded with *cos* functions in a length L_∞ surrounded by rigid walls; as follows [52]:

$$\phi_n(z) = \sqrt{\frac{2}{L_\infty}}\cos\left(\frac{n\pi z}{L_\infty} - \delta_n\right), \tag{9}$$

where $\delta_n = 0$ if n is old and $\delta_n = \pi/2$ if n is even. The wave functions of the structure are then described with a complete set of these base functions as $\psi(z) = \sum_{n=1}^{\infty} c_n\phi_n(z)$.

After getting the electronic wavefunctions and energy eigenvalues, optical properties can be calculated with the expressions obtained by the framework of the compact density matrix approach. In this paper, we wonder about the variations in the TOACs, RRICs, NORs, SHGs, and THGs. The relevant formulas for these coefficients cover transition energies between energy levels, dipole moment matrix elements associated with these levels, and some other physical terms which are given in the following. Although TOACs, RRICs, and NOR coefficients include the transitions only between the first two levels; SHG and THG comprises the transitions from the third level and third as well as fourth level to the ground state, respectively. Here, introducing the dipole moment matrix operator-$\widehat{M}_{ji}$ will be preferable. $\widehat{M}_{ji} = \left|\langle\psi_j(z)|ez|\psi_i(z)\rangle\right|$ with $i,\ j = 0,\ 1,\ 2,\ 3$ represents the spatial overlap between two wave functions for the first four states.

The analytical expressions for the total OAC -$\beta(\omega, I)$ and RRIC -$\frac{\Delta n(\omega, I)}{n_r}$ between the lowest-lying first two levels are given by [33–39]:

$$\beta(\omega, I) = \omega\sqrt{\frac{\mu_0}{\varepsilon_R}}\left\{\begin{array}{c}\left[\frac{|M_{10}|^2\rho_{01}\hbar\Gamma_{10}}{(\mathrm{E}_{10}-\hbar\omega)^2+(\hbar\Gamma_{10})^2}\right]- \\ \left[\left(\frac{I}{2cn_r\varepsilon_0}\right)\frac{|M_{10}|^2\rho_{01}\hbar\Gamma_{10}}{\left[(\mathrm{E}_{10}-\hbar\omega)^2+(\hbar\Gamma_{10})^2\right]^2}\left\{4|M_{10}|^2-\frac{|M_{11}-M_{00}|^2\left[3\mathrm{E}_{10}{}^2-4\mathrm{E}_{10}\hbar\omega+\hbar^2(\omega^2-\Gamma_{10}^2)\right]}{\mathrm{E}_{10}{}^2+(\hbar\Gamma_{10})^2}\right\}\right]\end{array}\right\}, \tag{10}$$

$$\frac{\Delta n(\omega, I)}{n_r} = \frac{\rho_{01}|M_{10}|^2}{2n_r^2\varepsilon_0}\times\left\{\begin{array}{c}\left[\frac{\mathrm{E}_{10}-\hbar\omega}{(\mathrm{E}_{10}-\hbar\omega)^2+(\hbar\Gamma_{10})^2}\right]-\frac{2\mu_0 cI}{\left[(\mathrm{E}_{10}-\hbar\omega)^2+(\hbar\Gamma_{10})^2\right]^2} \\ \times\left[4(\mathrm{E}_{10}-\hbar\omega)|M_{10}|^2-\frac{|M_{11}-M_{00}|^2}{\mathrm{E}_{10}{}^2+(\hbar\Gamma_{10})^2}\left[(\mathrm{E}_{10}-\hbar\omega)\left(\mathrm{E}_{10}(\mathrm{E}_{10}-\hbar\omega)-(\hbar\Gamma_{10})^2\right)-(\hbar\Gamma_{10})^2(2\mathrm{E}_{10}-\hbar\omega)\right]\right]\end{array}\right\} \tag{11}$$

where, ε_0 and μ_0 are the dielectric constant and permeability of the medium, respectively and ε_R is the real part of the permittivity. $\Gamma_{k0} = 1/\tau_{k0}$ is the relaxation rate term related to the inverse of electron's relaxation time (τ_{k0}), where $k = 1, 2, 3$. n_r specifies the system's refractive index, ω represents the frequency of incident photon energy while I specifies the strength of incident photon with the expression $I = (2n_r/\mu_0 c)|E(\omega)|^2$. ρ_{01} represents the density of intersubband transition electrons. $E_{k0} = (E_k - E_0)$ is the transition frequency between the initial (0) and final (k) states.

Other optical responses such as NOR ($\chi_0^{(2)}$), SHG ($\chi_{2\omega}^{(2)}$) and THG ($\chi_{3\omega}^{(3)}$) can be evaluated with the terms as below:

$$\chi_0^{(2)} = \frac{4e^3\rho_{01}}{\varepsilon_0\hbar^2}M_{10}^2\delta_{01}\frac{E_{10}^2(1+\Gamma_{20}/\Gamma_{10})+\hbar^2(\omega^2+\Gamma_{20}^2)(\Gamma_{20}/\Gamma_{10}-1)}{\left[(E_{10}-\hbar\omega)^2+\hbar^2\Gamma_{20}^2\right]\left[(E_{10}+\hbar\omega)^2+\hbar^2\Gamma_{20}^2\right]} \tag{12}$$

$$\chi_{2\omega}^{(2)} = \frac{e^3\rho_{01}}{\varepsilon_0}\frac{M_{10}M_{12}M_{20}}{(\hbar\omega-E_{10}-i\hbar\Gamma_{30})(2\hbar\omega-E_{20}-i\hbar\Gamma_{30}/2)} \tag{13}$$

$$\chi_{3\omega}^{(3)} = \frac{e^4\rho_{01}}{\varepsilon_0}\frac{M_{10}M_{12}M_{23}M_{30}}{(\hbar\omega-E_{10}-i\hbar\Gamma_{30})(2\hbar\omega-E_{20}-i\hbar\Gamma_{30}/2)(3\hbar\omega-E_{30}-i\hbar\Gamma_{30}/3)} \tag{14}$$

where δ_{01} is used to express the first two state diagonal dipole moment matrix differences and given as $|M_{00} - M_{11}|$.

3 Results and discussion

The energy levels and corresponding wave functions of an electron, confined within the conduction band of asymmetric triple potential wells formed between the interfaces of GaAs/$Al_{0.3}Ga_{0.7}As$ heterostructures and their related optical susceptibilities are displayed here. Furthermore, the sensitivities of these properties to the hydrostatic pressure and temperature are analyzed in detail. The numerical calculations are built with the following physical constants and fixed parameters: $e = 1.602\times10^{-19}$ C, $\hbar = 1.056\times10^{-34}$ Js, $\rho_{01} = 3\times10^{22}m^{-3}$, $n_r = 3.2$, $\mu_0 = 4\pi\times10^7 Hm^{-1}$, $\varepsilon_0 = 8.854\times10^{-12}Fm^{-1}$, $\Gamma_{10} = 1.0$THz, $\Gamma_{20} = 5.0$THz and $\Gamma_{30} = 7.0$THz and $I = 0.01MW/cm^2$. The width of the potential wells and barrier in the absence of hydrostatic pressure and temperature are $L_L = L_R = L_M = L_W = 100$ Å and $L_B = 20$ Å. The depth of potential with the zero external fields is $V_0 = 0.228eV$.

In Fig. 1, we displayed the distribution of potential function and lowest-lying first four energy levels and their corresponding wave function probabilities at the 300 K temperature. The upper parts of each well behave as a rectangular well while the bottom parts differ for each well. The bottom of the left well is a parabolic well, while the bottom of the right well behaves as an inverse parabolic well. The middle well includes adjacently placed semi-parabolic and inverse semi-parabolic wells. Ground state (red one) wave function probabilities of triple wells configuration locates almost all of itself in the left well due to strong confinement especially at the deeper sides of that well. The first excited state (blue one) occurs at comparatively higher energies and places itself in the middle well, because of stronger confinement for that energy level. At the lower energy states, the right well does not display robust confinement. However, the right well displays proper confinement for the higher energy level and so the most probabilities of the second excited state (pink one) settle down in the right well. The third excited state (green one) has probability distributions at all three wells because of the similar well configurations at the level of this energy state. Furthermore, the significant energy differences between levels can be noticeable in Fig. 1.

The expressions that relate the hydrostatic pressure and temperature to the effective mass, dielectric constant, barrier height, and well width were introduced in the theory section. The calculated values of these physical quantities for several pressures and temperatures are represented in Table 1. Effective mass and relative dielectric constant have an opposite responses to the changes in the pressure and temperature. The increment in the pressure, increases the effective mass and reduces the relative dielectric constant, while the temperature rises do exactly the opposite. As can be noticed from Table 1, the augmentation in both agents decreases the

Table 1 The changes in the effective mass (m^*), relative dielectric constant (ε), depth of the potential (V_0), and width of each well (L_w) while hydrostatic pressure and temperature are changing

p (kbar)	T (K)	m^* (m_0)	ε (ε_0)	V_0 (meV)	L_w (Å)
0	0	0.067	12.65	228	100
0	100	0.066	12.76	226	100
0	300	0.063	13.18	222	100
0	500	0.059	13.72	217	100
10	300	0.068	12.95	219	99.58
20	300	0.072	12.73	217	99.16
30	300	0.076	12.51	214	98.74

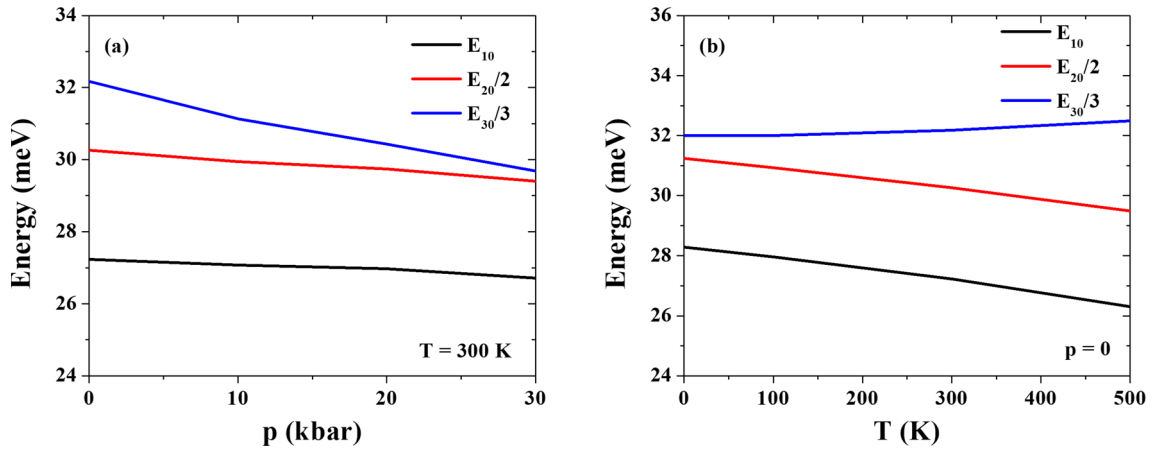

Fig. 2 Transition energies between the first three excited states and ground state as a function of hydrostatic pressure in (**a**) and temperature in (**b**)

depth of the barrier. Moreover, increases in pressure narrow the well widths; however, the changes in temperature do not act on them.

In Fig. 2, we presented the transition energies between levels while hydrostatic pressure and temperature are varying. Here, E_{10}, $E_{20}/2$, and $E_{30}/3$ stand for the transition energies from the first, second, and third excited states to the ground state, respectively. The effect of hydrostatic pressure on these energy differences is displayed in Fig. 2a and the impact of the temperature is drawn in Fig. 2b. Although increasing pressure values lead to little decreases in the transition energies between the first excited state → ground state (E_{10}) and the second excited state → ground state (E_{20}); it results in comparatively bigger transition energy changes for the passes from the third excited state to the ground state. This means that, the third excited state is more sensitive to the increases in the hydrostatic pressure than the ground and first excited states since its energy level is higher and its wavefunction was spread along the three wells as shown in Fig. 1. Furthermore, it can be noticed that the transition energies $E_{20}/2$ and $E_{30}/3$ become closer when the pressure values go to 30 kbar.

The effect of the rising temperature on the transition energies is more remarkable. Temperature rises decline the transition energy differences between the first two excited states and the ground state. Unlike the pressure augmentation case, the transition energy differences between the third excited state and ground state increase with the rising temperatures. In this case, the transition energies $E_{20}/2$ and $E_{30}/3$ present small differences at zero temperature; however, they present a significant split when T increases. In other words, the augmentation of the pressure and temperature present contrary effects on the $E_{30}/3$ transition energy.

From now on we will present the outcomes about the optical properties. Table 2 submits a quantitative representation of dipole moment matrix elements, which are the key elements on the optical coefficients with several hydrostatic pressure and temperature values. The column of M_{10} determines the magnitudes of TOAC and RRIC (see Eqs. 10, 11). Column of $M_{10}^2\delta_{01}$ specifies the NOR coefficients between the first excited state and the ground state. The column including the product of three dipole moment matrix elements ($M_{10}M_{12}M_{20}$) gives clues about the amplitude of SHG peaks. The last column of Table 2 includes four dipole moment matrix multiplication ($M_{10}M_{12}M_{23}M_{30}$) and forms the numerator part of the THG coefficient. Although increasing temperatures raise the values of all given dipole moment matrix elements , augmentation in the static pressure decreases them.

Figure 3a and b respectively show the changes in the TOACs while hydrostatic pressure and temperature are increasing. The peaks of TOACs slightly move to lower energies with decreasing amplitudes when the hydrostatic pressure increases. The rise in the temperatures also shifts the TOAC peaks to lower energies but with strengthened magnitudes. These redshifts in the peak energies can be attributed to the decreases in the E_{10} transition energy. The changes in the magnitudes of TOAC peaks can be correlated to the variations in the M_{10} dipole moment matrix element. The coherent variation attitudes are seen in Figs. 3, 4, and Table 2.

Table 2 The changes in the dipole moment matrix elements while hydrostatic pressure and temperature are increasing

p (kbar)	T (K)	M_{10} (Å)	$M_{10}^2\delta_{01}$ (Å)^3	$M_{10}M_{12}M_{20}$ (Å)^3	$M_{10}M_{12}M_{23}M_{30}$ (Å)^4
0	0	13.9648	25,046.8	1185.99	226,851
0	100	14.5735	27,124	1308.93	243,853
0	300	16.5848	35,165.3	1786.3	315,020
0	500	19.554	48,587.05	2646.05	430,132
0	300	16.5848	35,165.3	1786.3	315,020
10	300	14.8109	28,027.7	1357.7	251,122
20	300	13.583	23,532.7	1099.74	210,361
30	300	12.636	20,319.9	921.859	180,977

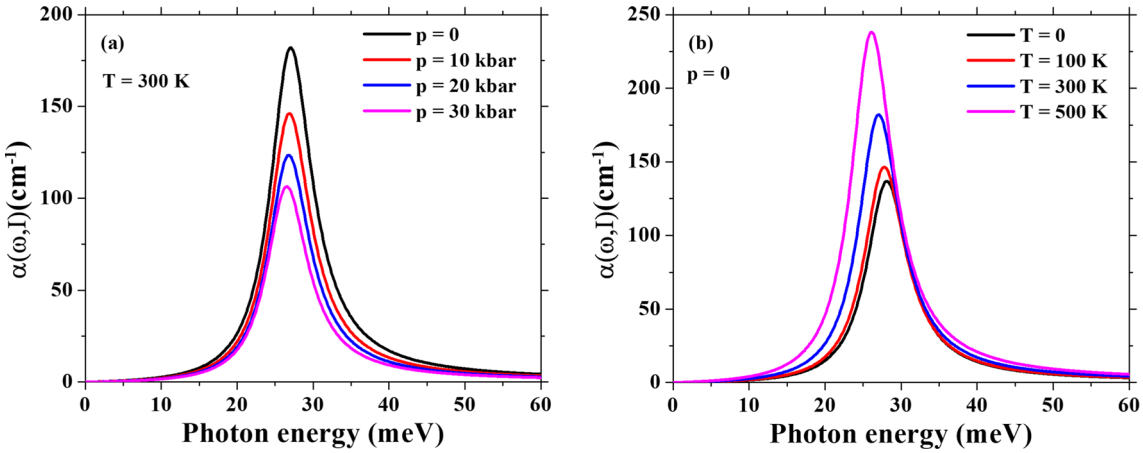

Fig. 3 Variations in the TOACs as a function of incident photon energy with the varying hydrostatic pressures in (**a**) and temperatures in (**b**)

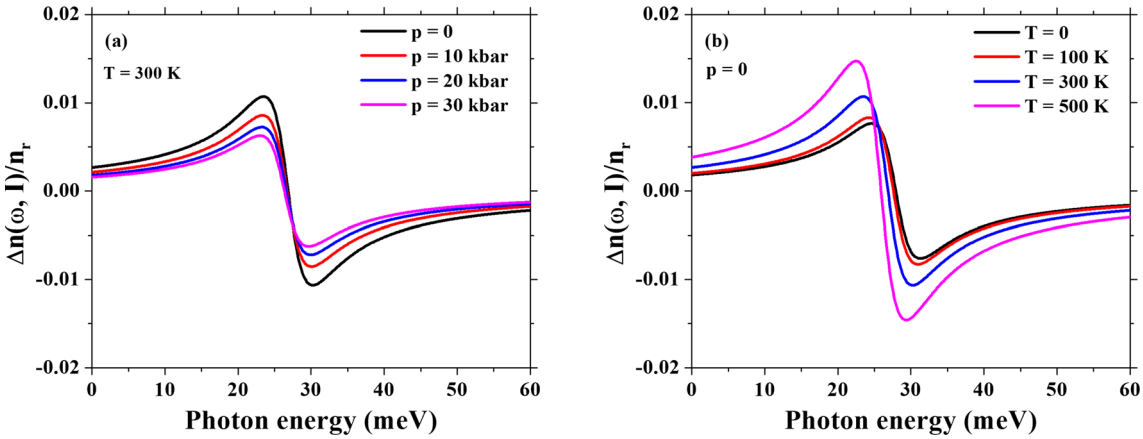

Fig. 4 Relative refractive index changes as a function of incident photon energies while hydrostatic pressure in (**a**) and temperature in (**b**) are increasing

The changes in the RRIC peaks with hydrostatic pressure and temperature are shown in Fig. 4. Increasing pressure slightly moves RRICs to the lower photon energies as seen in Fig. 4a. The rise in temperatures moves RRICs peaks to comparatively lower energies as drawn in Fig. 4b. Although the increase in hydrostatic pressure decreases the peak amplitudes of RRICs, the rise in temperature augments these peaks. The effects of hydrostatic pressure and temperature on the RRICs are in accordance with the responses of the TOACs served in Fig. 3. The findings once more imply that the influences of temperature are more pronounced than pressure within the studied values.

We present the modulations on the NOR coefficients with the increasing hydrostatic pressure in Fig. 5a and with temperature rise in Fig. 5b. The increase in pressure causes the peak position to shift to lower photon energies and the peak magnitudes decrease. The rise in temperature causes to redshift in the peaks and inclines the magnitudes. The alterations in the energy transitions between the first excited state and the ground state and the $M_{10}^2\delta_{01}(\text{Å})^3$ dipole moment matrix elements of these levels determine the character of the NOR coefficients.

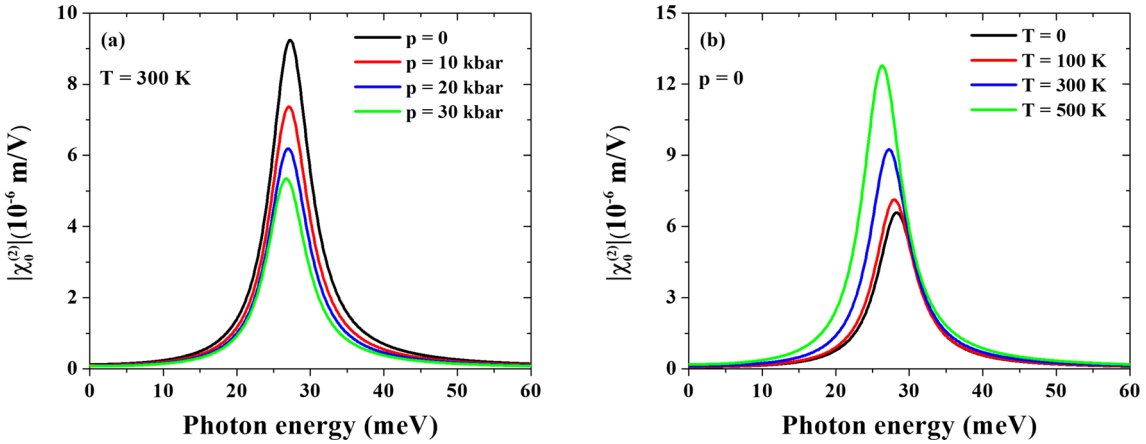

Fig. 5 Nonlinear optical rectification changes with respect to the incident photon energies as a function of hydrostatic pressure in (**a**) and temperature in (**b**)

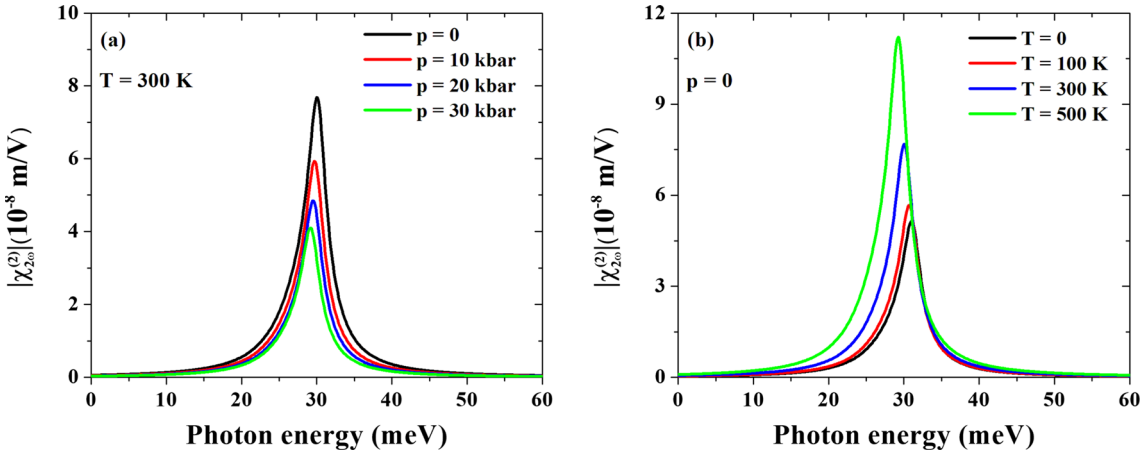

Fig. 6 The changes in the second harmonic generation coefficients with respect to the incident photon energies as a function of hydrostatic pressure in (**a**) and temperature in (**b**)

Figure 6 displays the responses of the SHG coefficients to the variations in the hydrostatic pressure and temperature, respectively. The variation behaviors of the primary peak of SHG is similar to the NOR characteristics. The slight shifts to red with decreasing magnitudes by pressure application and with increasing magnitudes by growing temperatures can be noticeable. The discrepancy between SHG and NOR peaks displays itself in the response to the different incident photon energies. SHG peaks occur at higher photon energies than NORs. The secondary peaks of SHG are not visible due to close transition energy values of E_{20} and E_{10}. In other words, the primary peaks suppress the emergence of secondary peaks because of the close energy differences.

The role of hydrostatic pressure and temperature on the third harmonic generation coefficients is drawn in Fig. 7. The significant redshift in the primary peaks and growing peak magnitudes with the augmented pressure are pictured in Fig. 7a. On the other side, rising temperatures reduce the primary peak magnitudes and cause slight shift toward higher energies. These magnitude changes with increasing pressure and temperature seem as a contrast to the last column of Table 2. The reason for that is the competition between the change rate of $M_{10}M_{12}M_{23}M_{30}$ and $E_{30}/3$. The change in transition energy is more dominant than the dipole moment matrix elements, it so suppresses the numerator term of THG coefficient. The secondary peaks of the THG become visible only at high temperatures such as 300 K and 500 K, when no pressure field is acting. This is again because of the closeness of transition energies between excited states and the ground state for each case. The transition energies associated with NOR, SHG, and THG coefficients vary in a narrow energy interval, as 26.3–32.5 meV.

4 Conclusion

The roles of the hydrostatic pressure and temperature on the electronic and optical properties of the asymmetric triple parabolic-like wells are examined. We first obtained the electronic wave functions and their energies by solving the Schrödinger equation within the effective mass and parabolic band approximations. Then, with the use of the compact density matrix approach, we have calculated the

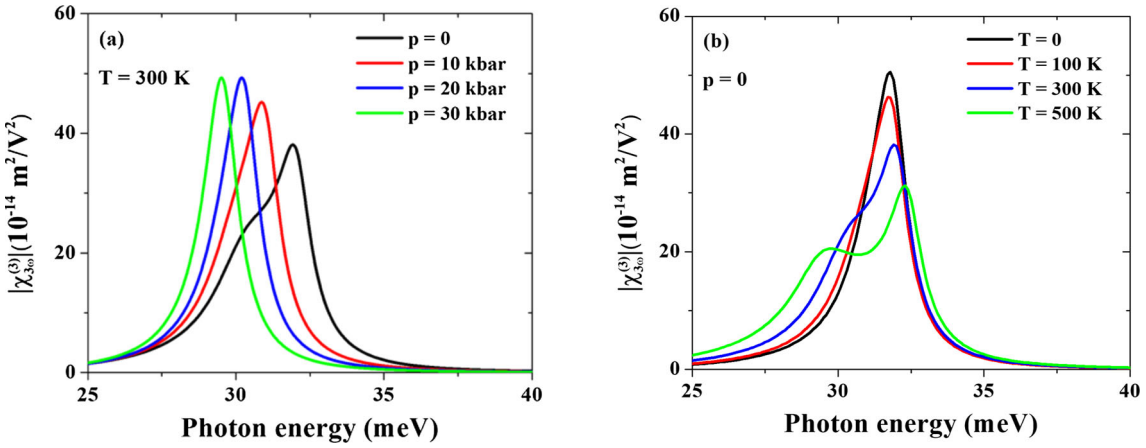

Fig. 7 Responses of third harmonic generation coefficients to the photon energy while pressure in (**a**) and temperature in (**b**) are changing

total optical absorption coefficients, relative refractive index changes, nonlinear optical rectification, and second and third harmonic generation coefficients. The increases in both the hydrostatic pressure and temperature lead redshift on these coefficients. The shifts of peak positions are slight when the hydrostatic pressure is increasing, but they are significant when the temperature is rising. On the other hand, the primary peaks of third harmonic generation display different attitude with the increases in the temperature by slightly moving to higher energies. Besides, the secondary peaks of third harmonic generation only become evident at high temperatures such as 300 K and 500 K, in the absence of pressure. The findings in this study imply that variations in temperature are more effective than hydrostatic pressure on the optical properties of this asymmetric triple QW system, for the discussed values. Tailoring electronic and optical properties with such type of asymmetric triple potential wells under solely hydrostatic pressure or temperature fields offers an additional degree of freedom. Therefore, we believe this study will contribute to the theoretical and experimental studies on light–matter interaction.

Data Availability Statement This manuscript has associated data in a data repository. [Authors' comment: No data associated with the manuscript.]

References

1. B. Chen, K.-X. Guo, R.-Z. Wang, Y.-B. Zheng, B. Li, Nonlinear optical rectification in asymmetric double triangular quantum wells. Eur. Phys. J. B. **66**, 227–233 (2008)
2. M.J. Karimi, A. Keshavarz, A. Poostforush, Linear and nonlinear intersub-band optical absorption and refractive index changes of asymmetric double semi-parabolic quantum wells. Superlattices Microstruct. **49**, 441–452 (2011)
3. S. Baskoutas, C. Garoufalis, A.F. Terzis, Linear and nonlinear optical absorption coefficients in inverse parabolic quantum wells under static external electric field. Eur. Phys. J. B. **84**, 241–247 (2011)
4. G. Liu, K. Guo, Q. Wu, Linear and nonlinear intersubband optical absorption and refractive index change in asymmetrical semi-exponential quantum wells. Superlattices Microstruct. **52**, 183–192 (2012)
5. N. Zeiri, N. Sfina, S. Abdi-Ben Nasrallah, M. Said, Linear and non-linear optical properties in symmetric and asymmetric double quantum wells. Optik **124**, 7044–7048 (2013)
6. C. Tang, J. Shi, Influence of delta doping on intersubband transition and absorption in AlGaN/GaN step quantum wells for terahertz applications. Physica E **69**, 96–100 (2015)
7. H. Dakhlaoui, Tunability of the optical absorption and refractive index changes in step-like and parabolic quantum wells under external electric field. Optik **168**, 416–423 (2018)
8. Z.-H. Zhang, J.-H. Yuan, K.-X. Guo, E. Feddi, Effect of conduction band non-parabolicity on the nonlinear optical properties in GaAs/$Ga_{1-x}Al_xAs$ double semi-V-shaped quantum wells. Materials **12**, 78 (2019)
9. H. Dakhlaoui, M. Nefzi, Tuning the linear and nonlinear optical properties in double and triple δ-doped GaAs semiconductor: Impact of electric and magnetic fields. Superlattices Microstruct. **136**, 106292 (2019)
10. H. Dakhlaoui, F. Ungan, J.C. Martínez-Orozco, M.E. Mora-Ramos, Theoretical investigation of linear and nonlinear optical properties in an heterostructure based on triple parabolic barriers: effects of external fields. Physica B **607**, 412782 (2021)
11. A. Ed-Dahmouny, N. Zeiri, R. Arraoui, N. Es-Sbai, M. Jaouane, A. Fakkahi, A. Sali, K. El-Bakkari, C.A. Duque, The third-order nonlinear optical susceptibility in an ellipsoidal core-shell quantum dot embedded in various dielectric surrounding matrices. Physica E **153**, 115784 (2023)
12. K. Ploog, Delta- (°-) doping in MBE-grown GaAs: concept and device application. J. Cryst. Growth **81**, 304–313 (1987)
13. D. Grützmacher, Growth and analysis of quantum well structures. J. Cryst. Growth **107**, 520–530 (1991)
14. N. Nanhui, W. Huaibing, L. Jianping, L. Naixin, X. Yanhui, H. Jun, D. Jun, S. Guangdi, Improved quality of InGaN/GaN multiple quantum wells by a strain relief layer. J. Cryst. Growth **286**, 209–212 (2006)
15. A. Ed-Dahmouny, R. Arraoui, M. Jaouane, A. Fakkahi, A. Sali, N. Es-Sbai, K. El-Bakkari, N. Zeiri, C.A. Duque, The influence of the electric and magnetic fields on donor impurity electronic states and optical absorption coefficients in a core/shell GaAs/Al0.33Ga0.67As ellipsoidal quantum dot. Eur Phys J Plus **138**, 774 (2023)
16. S.-R. Jeon, S.-J. Lee, S.H. Jung, S.H. Lee, J.H. Baek, H. Jeong, O.H. Cha, E.-K. Suh, M.S. Jeong, Effect of V-shaped defects on structural and optical properties of AlGaN/InGaN multiple quantum wells. J. Phys. D Appl. Phys. **41**, 132006 (2008)

17. C. Deimert, Z.R. Wasilewski, MBE growth of continuously-graded parabolic quantum well arrays in AlGaAs. J. Cryst. Growth **514**, 103–108 (2019)
18. A. Ed-Dahmouny, N. Zeiri, A. Fakkahi, R. Arraoui, M. Jaouane, A. Sali, N. Es--Sbai, K. El-Bakkari, C.A. Duque, Impurity photo-ionization cross section and stark shift of ground and two low-lying excited electron-states in a core/shell ellipsoidal quantum dot. Chem Phys. Lett. **812**, 140251 (2023)
19. A.M. Elabsy, Hydrostatic pressure dependence of binding energies for donors in quantum well heterostructures. Phys. Scr. **48**, 376–378 (1993)
20. A.J. Peter, K. Navaneethakrishnan, Simultaneous effects of pressure and temperature on donors in a GaAlAs/GaAs quantum well. Superlatt. Microstruct. **43**, 63–71 (2008)
21. H. Akbas, I. Erdogan, O. Akankan, Hydrostatic pressure effects on impurity states in GaAs/AlAs quantum wells. Superlatt. Microstruct. **50**, 80–89 (2011)
22. M.R. Fulla, Y.A. Suaza, J.H. Marın, Hydrostatic pressure, temperature and aluminum concentration effects on the ground state of coupled donors in a GaAs–Ga_{1-x} Al_xAs quantum well. Phys. Status Solidi B **252**, 678–682 (2015)
23. N. Eseanu, E.C. Niculescu, Hydrostatic pressure and temperature effects on the donor binding energy in asymmetrical square quantum wells. U.P.B. Sci. Bull Series A Appl. Math. Phys. **72**, 21–26 (2010)
24. N. Raigoza, A.L. Morales, C.A. Duque, Effects of hydrostatic pressure on donor states in symmetrical GaAs–Ga0.7Al0.3As double quantum wells. Physica B **363**, 262–270 (2005)
25. N. Eseanu, Simultaneous effects of laser field and hydrostatic pressure on the intersubband transitions in square and parabolic quantum wells. Phys. Lett. A **374**, 1278–1285 (2010)
26. M.G. Barseghyan, A. Hakimyfard, S.Y. Lopez, C.A. Duque, A.A. Kirakosyan, Simultaneous effects of hydrostatic pressure and temperature on donor binding energy and photoionization cross section in Pöschl-Teller quantum well. Physica E **42**, 1618–1622 (2010)
27. P. Baser, S. Elagoz, The hydrostatic pressure and temperature effects on hydrogenic impurity binding energies in lattice matched InP/In0.53Ga0.47As/InP square quantum well. Superlatt Microstruct **102**, 173–179 (2017)
28. E. Cicek, A.I. Mese, B. Ozkapi, I. Erdogan, Combined effects of the hydrostatic pressure and temperature on the self-polarization in a finite quantum well under laser field. Superlatt. Microstruct. **155**, 106904 (2021)
29. H.D. Karki, S. Elagoz, P. Baser, Simultaneous effects of hydrostatic pressure and temperature on the binding energy of hydrogenic impurity in cylindrical quantum well wires. Superlatt. Microstruct. **48**, 298–304 (2010)
30. E. Kasapoglu, The hydrostatic pressure and temperature effects on donor impurities in GaAs/$Ga_{1-x}Al_x$As double quantum well under the external fields. Phys. Lett. A **373**, 140–143 (2008)
31. H. Odhiambo Oyoko, N. Porras-Montenegro, S.Y. Lopez, C.A. Duque, Comparative study of the hydrostatic pressure and temperature effects on the impurity-related optical properties in single and double GaAs-$Ga_{1-x}Al_x$As quantum wells. Phys. Stat. Sol. (c) **4**, 298–300 (2007)
32. N. Raigoza, A.L. Morales, C.A. Duque, Infinite potential barrier and hydrostatic pressure effects on impurity-related optical absorption spectra in GaAs double quantum wells. Braz. J. Phys. **36**, 350–353 (2006)
33. M. Nazari, M.J. Karimi, A. Keshavarz, Linear and nonlinear optical absorption coefficients and refractive index changes in modulation-doped quantum wells: effects of the magnetic field and hydrostatic pressure. Physica B **428**, 30–35 (2013)
34. E. Ozturk, I. Sokmen, Nonlinear intersubband absorption and refractive index changes in square and graded quantum well modulated by temperature and hydrostatic pressure. J. Lumin. **134**, 42–48 (2013)
35. U. Yesilgul, F. Ungan, E.B. Al, E. Kasapoglu, H. Sari, I. Sokmen, Effects of magnetic field, hydrostatic pressure and temperature on the nonlinear optical properties in symmetric double semi-V-shaped quantum well. Opt. Quant. Electron. **48**, 560 (2016)
36. Z.-H. Zhang, L. Zou, K.-X. Guo, J.-H. Yuan, The effect of hydrostatic pressure, temperature and magnetic field on the nonlinear optical properties of asymmetrical Gaussian potential quantum wells. Physica E **77**, 90–96 (2016)
37. Z.-H. Zhang, J.-H. Yuan, K.-X. Guo, The combined influence of hydrostatic pressure and temperature on nonlinear optical properties of GaAs/Ga0.7Al0.3As morse quantum well in the presence of an applied magnetic field. Materials **11**, 668 (2018)
38. A.T. Tuzemen, H. Dakhlaoui, F. Ungan, Effects of hydrostatic pressure and temperature on the nonlinear optical properties of GaAs/GaAlAs zigzag quantum well. Phil. Mag. **102**, 2428–2443 (2022)
39. F. Ungan, R.L. Restrepo, M.E. Mora-Ramos, A.L. Morales, C.A. Duque, Intersubband optical absorption coefficients and refractive index changes in a graded quantum well under intense laser field: effects of hydrostatic pressure, temperature and electric field. Physica B **434**, 26–31 (2014)
40. F. Ungan, U. Yesilgul, S. Sakiroglu, M.E. Mora-Ramos, C.A. Duque, E. Kasapoglu, H. Sari, I. Sökmen, Simultaneous effects of hydrostatic pressure and temperature on the nonlinear optical properties in a parabolic quantum well under the intense laser field. Optics Communications **309**, 158–162 (2013)
41. F. Ungan, M.E. Mora-Ramos, H. Sari, I. Sökmen, Hydrostatic pressure and temperature effect on the electron-related optical responses in symmetric and asymmetric n-type double delta-doped gaas quantum well under terahertz laser field. J. Electron. Mater. **48**, 3537–3546 (2019)
42. M. Sayrac, A. Turkoglu, F. Ungan, Influence of hydrostatic pressure, temperature, and terahertz laser field on the electron-related optical responses in an asymmetric double quantum well. Eur. Phys. J. B. **94**, 121 (2021)
43. M.J. Karimi, A. Keshavarz, Second harmonic generation in asymmetric double semi-parabolic quantum wells: effects of electric and magnetic fields, hydrostatic pressure and temperature. Physica E **44**, 1900–1904 (2012)
44. X. Liu, L. Zou, C. Liu, Z.-H. Zhang, J.-H. Yuan, The nonlinear optical rectification and second harmonic generation in asymmetrical Gaussian potential quantum well: effects of hydrostatic pressure, temperature and magnetic field. Opt. Mater. **53**, 218–223 (2016)
45. J.-S. Li, Z.-H. Zhang, Y.-W. Liu, J.-H. Yuan, Simultaneous effects of hydrostatic pressure, temperature and aluminum concentration on nonlinear optical rectification, second- and third-harmonic generation in a GaAs/Ga1−xAlxAs morse quantum well. Int. J. Mod. Phys. B **33**, 1950009 (2019)
46. S.-R. Ge, X.-Y. Xu, W.-H. Zhang, Z.-Y. Song, Influence of temperature and hydrostatic pressure on the nonlinear optical properties in a GaAs/GaAlAs Kratzer-Fues confined quantum well. Physica E **143**, 115369 (2022)
47. R. Yahyazadeh, Numerical modeling of electronic and electrical characteristics of InGaN/GaN multiple quantum well solar cells. J. Photon. Energ. **10**, 045504 (2020)
48. M. Bajda, B. Piechal, F. Dybala, A. Bercha, W. Trzeciakowski, J.A. Majewski, Pressure and temperature dependence of gain in InGaAs/GaAs laser diode. Phys. Status Solidi B **249**, 217–221 (2012)
49. O. Oubram, L. Cisneros-Villalobos, M. Limón-Mendoza, F. A. Roblero, M. T. Torres, M. Abatal, The effects of the touch voltage and hydrostatic pressure on the optical absorption of delta-MIGFET transistor, In: *International Conference on Multimedia Computing and Systems (ICMCS)* 1426–1429 (2014)
50. Z.-H. Zhang, J.-H. Yuan, The third-order nonlinear optical susceptibility of Al_xGa_{1-x}As/GaAs asymmetric triple quantum wells. The Eur. Phys. J. Plus **137**, 1367 (2022)
51. R.F. Kopf, M.H. Herman, M. Lamont Schnoes, A.P. Perley, G. Livescu, M. Ohring, Band offset determination in analog graded parabolic and triangular quantum wells of GaAs/AlGaAs and GaInAs/AlInAs. J. Appl. Phys. **71**, 5004 (1992)
52. J.-B. Xia, W.-J. Fan, Electronic structures of superlattices under in-plane magnetic field. Phys. Rev. B **40**, 8508 (1989)